

Detecting the MSSM Higgs Bosons at Future e^+e^- Colliders

A. Gutiérrez-Rodríguez ¹, M. A. Hernández-Ruíz ² and O. A. Sampayo ³

(1) *Escuela de Física, Universidad Autónoma de Zacatecas
Apartado Postal C-580, 98060 Zacatecas, Zacatecas México.*

(2) *Facultad de Matemáticas, Universidad Autónoma de Zacatecas
Apartado Postal C-612, 98060 Zacatecas, Zacatecas México.*

(3) *Departamento de Física, Universidad Nacional del Mar del Plata
Funes 3350, (7600) Mar del Plata, Argentina.*

(November 18, 2018)

Abstract

We investigate the possibility of detecting the Higgs bosons predicted in the Minimal Supersymmetric extension of the Standard Model (h^0, H^0, A^0, H^\pm), with the reactions $e^+e^- \rightarrow b\bar{b}h^0(H^0, A^0)$, and $e^+e^- \rightarrow \tau^-\bar{\nu}_\tau H^+, \tau^+\nu_\tau H^-$, using the helicity formalism. We analyze the region of parameter space ($m_{A^0} - \tan\beta$) where h^0, H^0, A^0 and H^\pm could be detected in the limit when $\tan\beta$ is large. The numerical computation is done considering two stages of a possible Next Linear e^+e^- Collider: the first with $\sqrt{s} = 500 \text{ GeV}$ and design luminosity 50 fb^{-1} , and the second with $\sqrt{s} = 1 \text{ TeV}$ and luminosity $100\text{-}200 \text{ fb}^{-1}$.

PACS: 14.80.Cp, 12.60.Jv

I. INTRODUCTION

Higgs bosons [1] play an important role in the Standard Model (SM) [2]; they are responsible for generating the masses of all the elementary particles (leptons, quarks, and gauge bosons). However, the Higgs-boson sector is the least tested one in the SM. If Higgs bosons are responsible for breaking the symmetry from $SU(2)_L \times U(1)_Y$ to $U(1)_{EM}$, it is natural to expect that other Higgs bosons are also involved in breaking other symmetries at the grand-unification scale. One of the more attractive extensions of the SM is Supersymmetry (SUSY) [3], mainly because of its capacity to solve the naturalness and hierarchy problems while maintaining the Higgs bosons elementary.

The minimal supersymmetric extension of the Standard Model (MSSM) doubles the spectrum of particles of the SM and the new free parameters obey simple relations. The scalar sector of the MSSM [4] requires two Higgs doublets, thus the remaining scalar spectrum contains the following physical states: two CP-even Higgs scalar (h^0 and H^0) with $m_{h^0} \leq m_{H^0}$, one CP-odd Higgs scalar (A^0) and a charged Higgs pair (H^\pm), whose detection would be a clear signal of new physics. The Higgs sector is specified at tree-level by fixing two parameters, which can be chosen as the mass of the pseudoscalar m_{A^0} and the ratio of vacuum expectation values of the two doublets $\tan \beta = v_2/v_1$, then the mass m_{h^0} , m_{H^0} and m_{H^\pm} and the mixing angle of the neutral Higgs sector α can be fixed. However, since radiative corrections produce substantial effects on the predictions of the model [5], it is necessary to specify also the squark masses, which are assumed to be degenerated. In this paper, we focus on the phenomenology of the neutral CP-even and CP-odd scalar (h^0, H^0, A^0) and charged (H^\pm).

The search for these scalars has begun at LEP, and current low energy bound on their masses gives $m_{h^0}, m_{A^0} > 90 \text{ GeV}$ and $m_{H^\pm} > 120 \text{ GeV}$ for $\tan \beta > 1$ [6]. At e^+e^- colliders the signals for Higgs bosons are relatively clean and the opportunities for discovery and detailed study will be excellent. The most important processes for the production and detection of the neutral and charged Higgs bosons h^0, H^0, A^0 and H^\pm , are: $e^+e^- \rightarrow Z^* \rightarrow h^0, H^0 + Z^0$, $e^+e^- \rightarrow Z^* \rightarrow h^0, H^0 + A^0$, $e^+e^- \rightarrow \nu\bar{\nu} + W^{+*}W^{-*} \rightarrow \nu\bar{\nu} + h^0, H^0$ (the later is conventionally referred to as WW fusions), and $e^+e^- \rightarrow H^+H^-$ [7]; precise cross-section formulas appear in Ref. [8]. The main decay modes of the neutral Higgs particles are in general $b\bar{b}$ decays ($\sim 90\%$) and $\tau^+\tau^-$ decays ($\sim 10\%$) which are easy to detect experimentally at e^+e^- colliders [9–11]. Charged Higgs particles decay predominantly into $\tau\nu_\tau$ and $t\bar{b}$ pairs.

The Z^0h^0 production cross-section contains an overall factor $\sin^2(\beta - \alpha)$ which suppresses it in certain parameter regions (with $m_{A^0} < 100 \text{ GeV}$ and $\tan \beta$ large); fortunately the A^0h^0 production cross-section contains the complementary factor $\cos^2(\beta - \alpha)$. Hence the Z^0h^0 and A^0h^0 channels together are well suited to cover all regions in the $(m_{A^0} - \tan \beta)$ plane, provided that the *c.m.* energy is high enough for Z^0h^0 to be produced through the whole m_{h^0} mass range, and that an adequate event rate can be achieved. These conditions are already shown to be satisfied [9–11] for $\sqrt{s} = 500 \text{ GeV}$ with assumed luminosity 10 fb^{-1} , as is expected to be the case of the Next Linear e^+e^- Collider (NLC).

In previous studies, the two-body processes $e^+e^- \rightarrow h^0(H^0) + Z^0$ and $e^+e^- \rightarrow h^0(H^0) + A^0$ have been evaluated [8] extensively. However, the inclusion of three-body process $e^+e^- \rightarrow h^0(H^0) + b\bar{b}$ and $e^+e^- \rightarrow A^0 + b\bar{b}$ [12] at future e^+e^- colliders energies [13–15] is necessary in order to know its impact on the two-body mode processes and also to search for new

relations that could have a cleaner signature of the Higgs bosons production.

In the other hand the decay modes of the charged Higgs bosons determine the signatures in the detector. If $m_{H^\pm} > m_t + m_b$, the dominant decays modes are $t\bar{b}$, $\bar{t}b$ and $\tau^+\nu_\tau$, $\tau^-\bar{\nu}_\tau$. In some part of the parameter space also the decay $H^\pm \rightarrow W^\pm h^0$ is allowed. If $m_{H^\pm} < m_t + m_b$, the charged Higgs boson will decay mainly into $\tau^+\nu_\tau$, $\tau^-\bar{\nu}_\tau$.

For $m_{A^0} \leq m_{Z^0}$, and if 50 events criterion are adequate, the H^+H^- pair production will be kinematically allowed and easily observable [9–11,16–18]. For $m_{A^0} > 120 \text{ GeV}$, $e^+e^- \rightarrow H^+H^-$ must be employed for detection of the three heavy Higgs bosons. Assuming that SUSY decays are not dominant, and using the 50 event criterion H^+H^- can be detected up to $m_{H^\pm} = 230 \text{ GeV}$ [9–11,16–18], assuming $\sqrt{s} = 500 \text{ GeV}$.

The upper limits in the H^+H^- mode are almost entirely a function of the machine energy (assuming an appropriately higher integrated luminosity is available at a higher \sqrt{s}). Two recent studies [19,20] show that at $\sqrt{s} = 1 \text{ TeV}$, with an integrated luminosity of 200 fb^{-1} , H^+H^- detection would extended to $m_{A^0} \sim m_{H^\pm} \sim 450 \text{ GeV}$ even if substantial SUSY decays of these heavier Higgs are present.

In the present paper we study the production of SUSY Higgs bosons at e^+e^- colliders. We are interested in finding regions that could allow the detection of the SUSY Higgs bosons for the set parameter space $(m_{A^0} - \tan\beta)$. We shall discuss the neutral and charged Higgs bosons production $b\bar{b}h^0(H^0, A^0)$, and $\tau^-\bar{\nu}_\tau H^+$, $\tau^+\nu_\tau H^-$ in the energy range of a future e^+e^- colliders [13–15] for large values of the parameter $\tan\beta$, where one expects to have a high production. Since the coupling $h^0b\bar{b}$ is proportional to $\sin\alpha/\cos\beta$, the cross-section will receive a large enhancement factor when $\tan\beta$ is large. Similar situation occurs for H^0 , whose coupling with $b\bar{b}$ is proportional to $\cos\alpha/\cos\beta$. The couplings of A^0 with $b\bar{b}$ and of H^\pm with $\tau^-\bar{\nu}_\tau, \tau^+\nu_\tau$ are directly proportional to $\tan\beta$, thus the amplitudes will always grow with $\tan\beta$. We consider the complete set of Feynman diagrams at tree-level and use the helicity formalism [21–27] for the evaluation of the amplitudes. The results obtained for the three-body processes are compared with the dominant two-body mode reactions for the plane $(m_{A^0} - \tan\beta)$. Succintly, our aim in this work is to analyze how much the results of the Bjorken Mechanism [Fig. 1, (1.4)] would be enhanced by the contribution from the diagrams depicted in Figs. 1.1-1.3, 1.5 and 1.6 in which the SUSY Higgs bosons are radiated by a $b(\bar{b})$ quark. For the case of the charged Higgs bosons the two-body mode [Figs. 3.1 and 3.4] would be enhanced by the contribution from the diagrams depicted in Figs. 3.2, 3.3, and 3.5, in which the charged Higgs boson is radiated by a $\tau^-\bar{\nu}_\tau$ ($\tau^+\nu_\tau$) lepton.

Recently, it has been shown that for large values of $\tan\beta$ the detection of SUSY Higgs bosons is possible at FNAL and LHC [28]. In the papers cited in Ref. [28] the authors calculated the corresponding three-body diagrams for hadron collisions. They pointed out the importance of a large bottom Yukawa coupling at hadron colliders and showed that the Tevatron collider may be a good place for detecting SUSY Higgs bosons. In the case of the hadron colliders the three-body diagrams come from gluon fusion and this fact makes the contribution from these diagrams more important, due to the gluon abundance inside the hadrons. The advantage for the case of e^+e^- colliders is that the signals of the processes are cleaner.

This paper is organized as follows. We present in Sec. II the relevant details of the calculations. Sec. III contains the results for the processes $e^+e^- \rightarrow b\bar{b}h^0(H^0, A^0)$ and $e^+e^- \rightarrow \tau^-\bar{\nu}_\tau H^+, \tau^+\nu_\tau H^-$ at future e^+e^- colliders. Finally, Sec. IV contains our conclusions.

II. HELICITY AMPLITUDE FOR HIGGS BOSONS PRODUCTION

When the number of Feynman diagrams is increased, the calculation of the amplitude is a rather unpleasant task. Some algebraic forms [29] can be used in it to avoid manual calculation, but sometimes the lengthy printed output from the computer is overwhelming, and one can hardly find the required results from it. The CALKUL collaboration [30] suggested the Helicity Amplitude Method (HAM) which can simplify the calculation remarkably and hence make the manual calculation realistic.

In this section we describe in brief the evaluation of the amplitudes at tree-level, for $e^+e^- \rightarrow b\bar{b}h^0(H^0, A^0)$ and $e^+e^- \rightarrow \tau^-\bar{\nu}_\tau H^+, \tau^+\nu_\tau H^-$ using the HAM [21–27]. This method is a powerful technique for computing helicity amplitudes for multiparticle processes involving massless spin-1/2 and spin-1 particles. Generalization of this method that incorporates massive spin-1/2 and spin-1 particles, is given in Ref. [27]. This algebra is easy to program and more efficient than computing the Dirac algebra.

A Higgs boson h^0, H^0, A^0 , and H^\pm can be produced in scattering e^+e^- via the following processes:

$$e^+e^- \rightarrow b\bar{b}h^0, \quad (1)$$

$$e^+e^- \rightarrow b\bar{b}H^0, \quad (2)$$

$$e^+e^- \rightarrow b\bar{b}A^0, \quad (3)$$

$$e^+e^- \rightarrow \tau^-\bar{\nu}_\tau H^+, \tau^+\nu_\tau H^-. \quad (4)$$

The diagrams of Feynman, which contribute at tree-level to the different reaction mechanisms, are depicted in Figs. 1-3. Using the Feynman rules given by the Minimal Supersymmetric Standard Model (MSSM), as summarized in Ref. [8], we can write the amplitudes for these reactions [12]. For the evaluation of the amplitudes we have used the spinor-helicity technique of Xu, Zhang and Chang [22] (denoted henceforth by XZC), which is a modification of the technique developed by the CALKUL collaboration [30]. Following XZC, we introduce a very useful notation for the calculation of the processes (1)-(3) [12] and (4). The complete formulas of the processes (1)-(3) are given in Ref. [12]. For the case of process (4), we present the relevant details of the calculations.

Let us consider the process

$$e^-(p_1) + e^+(p_2) \rightarrow \{\tau^-(k_2) + \bar{\nu}_\tau(k_3) + H^+(k_1), \tau^+(k_2) + \nu_\tau(k_3) + H^-(k_1)\}, \quad (5)$$

in which the helicity amplitude is denoted by $\mathcal{M}[\lambda(e^-), \lambda(e^+), \lambda(\tau^\mp), \lambda(\nu_\tau)]$.

Due to charge invariance, the cross-sections for the production processes $e^-e^+ \rightarrow \tau^-\bar{\nu}_\tau H^+$ and $e^-e^+ \rightarrow \tau^+\nu_\tau H^-$ are exactly the same. One should thus calculate the cross-section of one of the two reactions and then multiply by a factor of two to take into account the charge conjugate final state. This will enormously simplify the Feynman diagrams as well as the amplitudes of transition. The Feynman diagrams for this process are shown in Fig. 3. From this figure it follows that the amplitudes that correspond to each graph are

$$\begin{aligned} \mathcal{M}_1 &= -iC_1 P_{H^-}(k_2 + k_3) P_Z(p_1 + p_2) T_1, \\ \mathcal{M}_2 &= iC_2 P_\tau(k_1 + k_3) P_Z(p_1 + p_2) T_2, \\ \mathcal{M}_3 &= -iC_3 P_\nu(k_1 + k_2) P_Z(p_1 + p_2) T_3, \end{aligned} \quad (6)$$

$$\begin{aligned}\mathcal{M}_4 &= -iC_4 P_{H^-}(k_2 + k_3) P_\gamma(p_1 + p_2) T_4, \\ \mathcal{M}_5 &= iC_5 P_\tau(k_1 + k_3) P_\gamma(p_1 + p_2) T_5,\end{aligned}$$

where

$$\begin{aligned}C_1 &= -\frac{g^3}{16\sqrt{2}} \frac{m_\tau}{m_W} \tan\beta \frac{\cos 2\theta_W}{\cos^2 \theta_W}, \\ C_2 &= \frac{g^3}{32\sqrt{2}} \frac{m_\tau}{m_W} \tan\beta \frac{1}{\cos^2 \theta_W}, \\ C_3 &= C_2, \\ C_4 &= \frac{g^3}{2\sqrt{2}} \frac{m_\tau}{m_W} \tan\beta \sin^2 \theta_W, \\ C_5 &= C_4,\end{aligned}\tag{7}$$

while the propagators are

$$\begin{aligned}P_{Z^0}(p_1 + p_2) &= \frac{(s - m_{Z^0}^2) + im_{Z^0}\Gamma_{Z^0}}{(s - m_{Z^0}^2)^2 + (m_{Z^0}\Gamma_{Z^0})^2}, \\ P_{H^\pm}(k_2 + k_3) &= \frac{(2k_2 \cdot k_3 - m_{H^\pm}^2) + im_H\Gamma_{H^\pm}}{(2k_2 \cdot k_3 - m_{H^\pm}^2)^2 + (m_{H^\pm}\Gamma_{H^\pm})^2}, \\ P_\tau(k_1 + k_3) &= \frac{1}{m_{H^\pm}^2 + 2k_1 \cdot k_3}, \\ P_\nu(k_1 + k_2) &= \frac{1}{m_{H^\pm}^2 + 2k_1 \cdot k_2}, \\ P_\gamma(p_1 + p_2) &= \frac{1}{s},\end{aligned}\tag{8}$$

where $s = (p_1 + p_2)^2$ and the corresponding tensors are

$$\begin{aligned}T_1^\mu &= \bar{u}(k_2)(1 - \gamma_5)v(k_3)\bar{v}(p_2)(\not{k}_1 - \not{k}_2 - \not{k}_3)(v_e^z - a_e^z\gamma_5)u(p_1), \\ T_2^\mu &= \bar{u}(k_2)\gamma^\mu(v_e^z - a_e^z\gamma_5)(\not{k}_1 + \not{k}_3)(1 - \gamma_5)v(k_3)\bar{v}(p_2)\gamma_\mu(v_e^z - a_e^z\gamma_5)u(p_1), \\ T_3^\mu &= \bar{u}(k_2)(1 - \gamma_5)(\not{k}_1 + \not{k}_2)\gamma_\mu(v_\nu^z - a_\nu^z\gamma_5)v(k_3)\bar{v}(p_2)\gamma^\mu(v_e^z - a_e^z\gamma_5)u(p_1), \\ T_4^\mu &= \bar{u}(k_2)(1 - \gamma_5)v(k_3)\bar{v}(p_2)(\not{k}_1 - \not{k}_2 - \not{k}_3)u(p_1), \\ T_5^\mu &= \bar{u}(k_2)\gamma_\mu(\not{k}_1 + \not{k}_3)(1 - \gamma_5)v(k_3)\bar{v}(p_2)\gamma^\mu u(p_1).\end{aligned}\tag{9}$$

In fact, we rearrange the tensors T 's in such a way that they become appropriate to a computer program. Then, following the rules from helicity calculus formalism [21–27] and using identities of the type

$$\{\bar{u}_\lambda(p_1)\gamma^\mu u_\lambda(p_2)\}\gamma_\mu = 2u_\lambda(p_2)\bar{u}_\lambda(p_1) + 2u_{-\lambda}(p_1)\bar{u}_{-\lambda}(p_2),\tag{10}$$

which is in fact the so called Chisholm identity, and

$$\not{p} = u_\lambda(p)\bar{u}_\lambda(p) + u_{-\lambda}(p)\bar{u}_{-\lambda}(p),\tag{11}$$

defined as a sum of the two projections $u_\lambda(p)\bar{u}_\lambda(p)$ and $u_{-\lambda}(p)\bar{u}_{-\lambda}(p)$.

The spinor products are given by

$$\begin{aligned} s(p_i, p_j) &\equiv \bar{u}_+(p_i)u_-(p_j) = -s(p_j, p_i), \\ t(p_i, p_j) &\equiv \bar{u}_-(p_i)u_+(p_j) = [s(p_j, p_i)]^*. \end{aligned} \quad (12)$$

Using Eqs. (10)-(12), which are proved in Ref. [27], we can reduce many amplitudes to expressions involving only spinor products.

Evaluating the tensors of Eq. (9) for each combination of (λ, λ') with $\lambda, \lambda' = \pm 1$ one obtains the following expressions:

$$\begin{aligned} \mathcal{M}_1(+, +) &= F_1 f_1^{+,+} s(k_2, k_3) [s(p_2, k_1)t(k_1, p_1) - s(p_2, k_2)t(k_2, p_1) - s(p_2, k_3)t(k_3, p_1)], \\ \mathcal{M}_1(-, +) &= F_1 f_1^{-,+} s(k_2, k_3) [t(p_2, k_1)s(k_1, p_1) - t(p_2, k_2)s(k_2, p_1) - t(p_2, k_3)s(k_3, p_1)], \end{aligned} \quad (13)$$

$$\begin{aligned} \mathcal{M}_2(+, +) &= F_2 f_2^{+,+} s(k_2, p_2)t(p_1, k_1)s(k_1, k_3), \\ \mathcal{M}_2(-, +) &= F_2 f_2^{-,+} s(k_2, p_1)t(p_2, k_1)s(k_1, k_3), \end{aligned} \quad (14)$$

$$\begin{aligned} \mathcal{M}_3(+, +) &= F_3 f_3^{+,+} s(k_2, k_1)t(k_1, p_1)s(p_2, k_3), \\ \mathcal{M}_3(-, +) &= F_3 f_3^{-,+} s(k_2, k_1)t(k_1, p_2)s(p_1, k_3), \end{aligned} \quad (15)$$

$$\begin{aligned} \mathcal{M}_4(+, +) &= F_4 s(k_2, k_3) [s(p_2, k_1)t(k_1, p_1) - s(p_2, k_2)t(k_2, p_1) - s(p_2, k_3)t(k_3, p_1)], \\ \mathcal{M}_4(-, +) &= F_4 s(k_2, k_3) [t(p_2, k_1)s(k_1, p_1) - t(p_2, k_2)s(k_2, p_1) - t(p_2, k_3)s(k_3, p_1)], \end{aligned} \quad (16)$$

$$\begin{aligned} \mathcal{M}_5(+, +) &= F_5 s(k_2, p_2)t(p_1, k_1)s(k_1, k_3), \\ \mathcal{M}_5(-, +) &= F_5 s(k_2, p_1)t(p_2, k_1)s(k_1, k_3), \end{aligned} \quad (17)$$

where

$$\begin{aligned} F_1 &= -2iC_1 P_{H^\pm}(k_2 + k_3)P_{Z^0}(p_1 + p_2), \\ F_2 &= 4iC_2 P_\tau(k_1 + k_3)P_{Z^0}(p_1 + p_2), \\ F_3 &= -4iC_3 P_\nu(k_1 + k_2)P_{Z^0}(p_1 + p_2), \\ F_4 &= -2iC_4 P_{H^\pm}(k_2 + k_3)P_\gamma(p_1 + p_2), \\ F_5 &= 4iC_5 P_\tau(k_1 + k_3)P_\gamma(p_1 + p_2), \end{aligned} \quad (18)$$

and

$$\begin{aligned} f_1^{+,+} &= (v_e^z - a_e^z), \\ f_1^{-,+} &= (v_e^z + a_e^z), \\ f_2^{+,+} &= (v_e^z - a_e^z)^2, \\ f_2^{-,+} &= ((v_e^z)^2 - (a_e^z)^2), \\ f_3^{+,+} &= (v_\nu^z + a_\nu^z)(v_e^z - a_e^z), \\ f_3^{-,+} &= (v_\nu^z + a_\nu^z)(v_e^z + a_e^z). \end{aligned}$$

Here, $v_e^z = -1 + 4\sin^2\theta_W$, $a_e^z = -1$, $v_\nu^z = 1$ and $a_\nu^z = 1$, according to the experimental data [6].

After the evaluation of the amplitudes of the corresponding diagrams, we obtain the cross-sections of the analyzed processes for each point of the phase space using Eqs. (13)-(17) by a computer program, which makes use of the subroutine RAMBO (Random Momenta

Beautifully Organized). The advantages of this procedure in comparison to the traditional “trace technique” are discussed in Refs. [21–27].

We use the Breit-Wigner propagators for the Z^0 , h^0 , H^0 , A^0 and H^\pm bosons. The mass of the bottom ($m_b \approx 4.5\text{GeV}$) the mass ($M_{Z^0} = 91.2\text{GeV}$) and width ($\Gamma_{Z^0} = 2.4974\text{GeV}$) of Z^0 have been taken as inputs; the widths of h^0 , H^0 , A^0 and H^\pm are calculated from the formulas given in Ref. [8]. In the next sections we present the numerical computation of the processes $e^+e^- \rightarrow b\bar{b}h$, $h = h^0, H^0, A^0$ and $e^+e^- \rightarrow \tau^-\bar{\nu}_\tau H^+, \tau^+\nu_\tau H^-$.

III. DETECTION OF MSSM HIGGS BOSONS AT FUTURE POSITRO-ELECTRON COLLIDERS ENERGIES

In this paper, we study the detection of neutral and charged MSSM Higgs bosons at e^+e^- colliders, including three-body mode diagrams [Figs. 1.1-1.3, 1.5, and 1.6; Figs. 2.1-2.3, 2.5 and 2.6; Figs. 3.2, 3.3, and 3.5] besides the dominant mode diagram [Fig. 1.4; Fig. 2.4; Figs. 3.1, and 3.4] consider two stages of a possible Next Linear e^+e^- Collider: the first with $\sqrt{s} = 500\text{ GeV}$ and design luminosity 50 fb^{-1} , and the second with $\sqrt{s} = 1\text{ TeV}$ and luminosity $100\text{-}200\text{ fb}^{-1}$. We consider the complete set of Feynman diagrams (Figs. 1-3) at tree-level and utilize the helicity formalism for the evaluation of their amplitudes. In the next subsections, we present our results for the case of the different Higgs bosons.

A. Detection of h^0

In order to illustrate our results on the detection of the h^0 Higgs boson, we present graphs in the parameters space region $(m_{A^0} - \tan\beta)$, assuming $m_t = 175\text{ GeV}$, $M_{\tilde{t}} = 500\text{ GeV}$ and $\tan\beta > 1$ for NLC. Our results are displayed in Fig. 4, for $e^+e^- \rightarrow (A^0, Z^0) + h^0$ dominant mode and for the processes at three-body $e^+e^- \rightarrow b\bar{b}h^0$.

The total cross-section for each contour is 0.03 pb , and 0.01 pb , which gives 1500 events, and 500 events to an integrated luminosity of $\mathcal{L} = 50\text{ fb}^{-1}$. We can see from this figure, that the effect of the reaction $b\bar{b}h^0$ is not more important that $(A^0, Z^0) + h^0$, for most of the $(m_{A^0} - \tan\beta)$ parameter space regions. Nevertheless, there are substantial portions of parameter space in which the discovery of the h^0 is not possible using either $(A^0, Z^0) + h^0$ or $b\bar{b}h^0$.

For the case of $\sqrt{s} = 1\text{ TeV}$, the results of the detection of the h^0 are shown in Fig. 5. It is clear from this figure that the contribution of the process $e^+e^- \rightarrow b\bar{b}h^0$ becomes dominant, namely $e^+e^- \rightarrow (A^0, Z^0) + h^0$ is small in all parameter space. However, they could provide important information on the Higgs bosons detection. For instance, we give the contours for the total cross-section to, say 0.01 pb , 0.005 , and 0.003 pb for both processes. These cross-sections give 1000 events, 500 events, and 300 events in total to a integrated luminosity of $\mathcal{L} = 100\text{ fb}^{-1}$. While for $\mathcal{L} = 200\text{ fb}^{-1}$ the events number is 2000, 1000, and 600, respectively, then it will be detectable the h^0 at future e^+e^- colliders.

B. Detection of H^0

To illustrate our results regarding the detection of the heavy Higgs bosons H^0 , we give the contours for the total cross-section for both processes $e^+e^- \rightarrow (A^0, Z^0) + H^0$, $e^+e^- \rightarrow b\bar{b}H^0$ in Fig. 6 for $\sqrt{s} = 500 \text{ GeV}$ and $\mathcal{L} = 50 \text{ fb}^{-1}$. The contours for this cross-section are 0.01 pb, 0.001 pb and 0.0001 pb for both reactions $(A^0, Z^0) + H^0$ and $b\bar{b}H^0$. The number of events corresponding to each contour are 500, 50 and 5, respectively.

Our estimate is that if more than 100 total events are obtained for a given process $(A^0, Z^0) + H^0$ or $b\bar{b}H^0$ then the Higgs boson H^0 can be detectable.

For the case of $\sqrt{s} = 1 \text{ TeV}$, the results on the detection of the H^0 are show in Fig. 7. The events number for each contour is 1000, 100, and 10 for $\mathcal{L} = 100 \text{ fb}^{-1}$ and 2000, 200, 20 for $\mathcal{L} = 200 \text{ fb}^{-1}$.

The effect of incorporate $b\bar{b}H^0$ in the detection of the Higgs boson H^0 is more important than the case of two-body mode $(A^0, Z^0) + H^0$, because $b\bar{b}H^0$ cover a major region in the parameters space $(m_{A^0} - \tan\beta)$. The most important conclusion from this figure is that detection of all of the neutral Higgs bosons will be possible at Next Linear e^+e^- Collider.

C. Detection of A^0

For the pseudoscalar A^0 , it is interesting to consider the production mode in $b\bar{b}A^0$, since it can have large a cross-section due to the fact that the coupling of A^0 with $b\bar{b}$ is directly proportional to $\tan\beta$, thus will always grow with it. In Fig. 8, we present the contours of the cross-sections for the process of our interest $b\bar{b}A^0$, at $\sqrt{s} = 500 \text{ GeV}$ and $\mathcal{L} = 50 \text{ fb}^{-1}$.

We display the contour lines for $\sigma = 0.01, 0.003, 0.001$, showing also the regions where the A^0 can be detected. These cross-sections give a contour of production of 500, 150 and 50 events. It is clear from this figure that very high experimental and analysis efficiencies are necessary for detecting the Higgs boson A^0 .

On the other hand, if we focus the detection of the A^0 at $\sqrt{s} = 1 \text{ TeV}$ and an integrated luminosity of $\mathcal{L} = 100 \text{ fb}^{-1}$, the panorama for its detection is more extensive. The Fig. 9 shows the contours lines in the plane $(m_{A^0} - \tan\beta)$, to the cross-section of $b\bar{b}A^0$. The contours for this cross-section correspond to 300, 100 and 10 events. While for $\mathcal{L} = 200 \text{ fb}^{-1}$ we have 600, 200, and 20 events respectively. It is estimated that if more than 100 total events are obtained for $b\bar{b}A^0$, then it is possible to detect the A^0 .

D. Detection of H^\pm

Our results for the H^+H^- scalars are displayed in Fig. 10, 11 for $e^+e^- \rightarrow H^+H^-$ dominant mode and for the processes at three-body $e^+e^- \rightarrow \tau^-\bar{\nu}_\tau H^+, \tau^+\nu_\tau H^-$.

The total cross-section for this reaction with $\sqrt{s} = 500 \text{ GeV}$ and $\mathcal{L} = 50 \text{ fb}^{-1}$ are shown in Fig. 10 for each contour with 0.01, 0.001, and 0.0001 pb, which gives 500 events, 50 events, and 5 events, respectively. We can see from this figure that the effect of the reactions $\tau^-\bar{\nu}_\tau H^+$ and $\tau^+\nu_\tau H^-$ is slightly more important than H^+H^- for most of the $(m_{A^0} - \tan\beta)$ parameters space regions. Nevertheless, there are substantial portions of parameters space in which the discovery of the H^\pm is not possible using either H^+H^- or $\tau^-\bar{\nu}_\tau H^+$ and $\tau^+\nu_\tau H^-$.

In both cases the curves with values of 0.01 pb , 0.001 pb , and 0.0001 pb give 1000, 100, and 10 events to an integrated luminosity of $\mathcal{L} = 100 \text{ fb}^{-1}$. Meanwhile, for $\mathcal{L} = 200 \text{ fb}^{-1}$ we have 2000, 200, and 20 events. These cross-sections are small, however, it is precisely in this curve where the contribution of the processes at three-body is notable. The most important conclusion from this figure is that detection of the charged Higgs bosons will be possible at future e^+e^- colliders.

IV. CONCLUSIONS

In this paper, we have calculated the production of the neutral and charged Higgs bosons in association with b -quarks and with $\tau\nu_\tau$ leptons via the processes $e^+e^- \rightarrow b\bar{b}h$, $h = h^0, H^0, A^0$ and $e^+e^- \rightarrow \tau^-\bar{\nu}_\tau H^+, \tau^+\nu_\tau H^-$ using the helicity formalism. We find that these processes could help to detect the possible neutral and charged Higgs bosons at energies of a possible Next Linear e^+e^- Collider when $\tan\beta$ is large.

In summary, we conclude that the possibilities of detecting or excluding the neutral and charged Higgs bosons of the Minimal Supersymmetric Standard Model (h^0, H^0, A^0, H^\pm) in the processes $e^+e^- \rightarrow b\bar{b}h$, $h = h^0, H^0, A^0$ and $e^+e^- \rightarrow \tau^-\bar{\nu}_\tau H^+, \tau^+\nu_\tau H^-$ are important and in some cases are compared favorably with the dominant mode $e^+e^- \rightarrow (A^0, Z^0) + h$, $h = h^0, H^0, A^0$ and $e^+e^- \rightarrow H^+H^-$ in the region of parameters space ($m_{A^0} - \tan\beta$) with $\tan\beta$ large. The detection of the Higgs boson will require the use of a future high energy machine like the Next Linear e^+e^- Collider.

Acknowledgments

This work was supported in part by *Consejo Nacional de Ciencia y Tecnología* (CONA-CyT) (Proyecto I33022-E) and *Sistema Nacional de Investigadores* (SNI) (México). A.G.R. would like to thank the organizers of the Summer School in Particle Physics 99, Trieste Italy for their hospitality. O. A. S. would like to thank CONICET (Argentina).

FIGURE CAPTIONS

Fig. 1 Feynman Diagrams at tree-level for $e^+e^- \rightarrow b\bar{b}h^0$. For $e^+e^- \rightarrow b\bar{b}H^0$ one has to make only the change $\sin\alpha/\cos\beta \rightarrow \cos\alpha/\cos\beta$.

Fig. 2 Feynman Diagrams at tree-level for $e^+e^- \rightarrow b\bar{b}A^0$.

Fig. 3 Feynman Diagrams at tree-level for $e^+e^- \rightarrow \tau^-\bar{\nu}_\tau H^+, \tau^+\nu_\tau H^-$.

Fig. 4 Total cross-sections contours in $(m_{A^0} - \tan\beta)$ parameter space for $e^+e^- \rightarrow (A^0, Z^0) + h^0$ and $e^+e^- \rightarrow b\bar{b}h^0$ with $\sqrt{s} = 500 \text{ GeV}$ and an integrated luminosity of $\mathcal{L} = 50 \text{ fb}^{-1}$. We have taken $m_t = 175 \text{ GeV}$ and $M_{\tilde{t}} = 500 \text{ GeV}$ and neglected squark mixing.

Fig. 5 Total cross-sections contours for $\sqrt{s} = 1 \text{ TeV}$ and $\mathcal{L} = 100, 200 \text{ fb}^{-1}$. We have taken $m_t = 175 \text{ GeV}$, $M_{\tilde{t}} = 500 \text{ GeV}$ and neglected squark mixing. We display contours for $e^+e^- \rightarrow (A^0, Z^0) + h^0$ and $e^+e^- \rightarrow b\bar{b}h^0$, in the parameters space $(m_{A^0} - \tan\beta)$.

Fig. 6 Same as in Fig. 4, but for $e^+e^- \rightarrow (A^0, Z^0) + H^0$ and $e^+e^- \rightarrow b\bar{b}H^0$.

Fig. 7 Same as in Fig. 5, but for $e^+e^- \rightarrow (A^0, Z^0) + H^0$ and $e^+e^- \rightarrow b\bar{b}H^0$.

Fig. 8 Same as in Fig. 4, but for $e^+e^- \rightarrow b\bar{b}A^0$.

Fig. 9 Same as in Fig. 5, but for $e^+e^- \rightarrow b\bar{b}A^0$.

Fig. 10 Same as in Fig. 4, but for $e^+e^- \rightarrow H^+H^-$ and $e^+e^- \rightarrow \tau^-\bar{\nu}_\tau H^+, \tau^+\nu_\tau H^-$.

Fig. 11 Same as in Fig. 5, but for $e^+e^- \rightarrow H^+H^-$ and $e^+e^- \rightarrow \tau^-\bar{\nu}_\tau H^+, \tau^+\nu_\tau H^-$.

REFERENCES

- [1] P. W. Higgs, Phys. Lett. **12**, (1964) 132; P. W. Higgs, Phys. Rev. Lett. **13**, (1964) 508; P. W. Higgs, Phys. Rev. Lett. **145**, (1966) 1156; F. Englert, R. Brout, Phys. Rev. Lett. **13**, (1964) 321; G. S. Guralnik, C. S. Hagen, T. W. B. Kibble, Phys. Rev. Lett. **13** (1964), 585.
- [2] S. Weinberg, Phys. Rev. Lett. **19**, (1967) 1264; A. Salam, in *Elementary Particle Theory*, ed. N. Southholm (Almquist and Wiksell, Stockholm, 1968), p.367; S.L. Glashow, Nucl. Phys. **22**, (1967) 257.
- [3] H. P. Nilles, Phys. Rep. **110**, (1984) 1; H. Haber and G. L. Kane, Phys. Rep. **117**, (1985) 75.
- [4] J. F. Gunion and H. E. Haber, Nucl. Phys. **B272**, (1986) 1; Nucl. Phys. **B278**, (1986) 449; Nucl. Phys. **B307**, (1988) 445; erratum *ibid.* **B402**, (1993) 567.
- [5] S.P. Li and M. Sher, phys. Lett. **B149**, (1984) 339; J. F. Gunion and A. Turski, Phys. Rev. **D39**, (1989) 2701; **40**, (1989) 2325; **40**, (1989) 2333; Y. Okada *et al.* Prog. Theor. Phys. Lett. **85**, (1991) 1; H. Haber and R. Hempfling, Phys. Rev. Lett. **66**, (1991) 1815; J. Ellis *et al.*, Phys. Lett. **B257**, (1991) 83; M. Dress and M. N. Nojiri, Phys. Rev. **D45**, (1992) 2482; M. A. Diaz and H. E. Haber, Phys. Rev. **D45**, (1992) 4246; D. M. Pierce, A. Papadoupoulos and S. Jonhson, Phys. Rev. Lett. **68**, (1992) 3678; P. H. Chankowski, S. Poporski and J. Rosiek, Phys. Lett. **B274**, (1992) 191; A. Yamada, Mod. Phys. Lett. **A7**, (1992) 2877.
- [6] Review of Particle Physics, D. Haidt, P. M. Zerwas, Euro. Phys. J. **C3**, (1998) 244.
- [7] S. Komamiya, Phys. Rev. **D38**, (1988) 2158.
- [8] For a recent review see J. Gunion, H. Haber, G. Kane and S. Dowson, *The Higgs Hunter's Guide* (Addison-Wesley, Reading, MA, 1990).
- [9] P. Janot, Orsay Report No. LAL 91-61, 1991 (unpublished); J-F Grivas, Orsay Report No. LAL 91-63, 1991 (unpublished) A. Brignole, J. Ellis, J. F. Gunion, M. Guzzo, F. Olmes, G. Ridolfi, L. Roszkowski and F. Zwirner, in *e^+e^- Collision at 500 GeV: The Physics Potential*, Munich, Annecy, Hamburg Workshop, DESY 92-123A, DESY 92-123B, DESY 93-123C, ed. P. Zerwas, p. 613; A. Djouadi, J. Kalinowski, P. M. Zerwas, *ibid.*; p.83 and Z. Phys. **C57**, (1993) 56; and references therein; *Physics and Technology of the Next Linear: a Report Submitted to Snowmass 1996*, BNL 52-502, FNAL-PUB-96/112, LBNL-PUB-5425, SLAC Report 485, UCRL-JD-124160.
- [10] M. Carena and P. M. Zerwas, Working Group, hep-ph/9602250, and references therein; S. Moretti and W. J. Stirling, Phys. Lett. **B347**, (1995) 291; Erratum, *ibidem* **B366**, (1996) 451. J. F. Gunion, *Detection and Studying Higgs Bosons*, hep-ph/9705282, UCD-97-13, 1997;
- [11] Andre Sopczak, Z. Phys. **C65**, (1995) 449; A. Sopczak, hep-ph/9712283, IEKP-KA/97-14, 1997; Stefano Moretti and Kosuke Odagiri, hep-ph/9612367; S. Moretti and K. Odagiri, Eur. Phys. J. **C1**, (1998) 633; E. Accomando, *et al.* Phys. Rep. **299**, (1998) 1.
- [12] U. Cotti, A. Gutiérrez-Rodríguez, A. Rosado and O. A. Sampayo, Phys. Rev. **D59**, (1999) 095011.
- [13] NLC ZDR Desing Group and the NLC Physics Working Group, S. Kuhlman *et al.*, *Physics and Technology of the Next Linear Collider*, hep-ex/9605011.
- [14] The NLC Design Group, C. Adolphsen *et al.* Zeroth-Order Design Report for the *Next Linear Collider*, LBNL-PUB-5424, SLAC Report No. 474, UCRL-ID-124161 (1996).

- [15] JLC Group, JLC-I, KEK Report No. 92-16, Tsukuba (1992).
- [16] A. Dejouadi *et al.*, hep-ph/9605437
- [17] A. Brignole, J. Ellis, J. F. Gunion, M. Guzzo, F. Olness, G. Ridolfi, L. Roszkowski and F. Zwirner, in e^+e^- **Collisions at 500 GeV: The Physics Potential**, Munich, Annecy, Hamburg Workshop, DESY 92-123A, DESY 92-123B, DESY 93-123C, ed. P. Zerwas, p. 163; A. Dejouadi, Kalinowski, P. M. Zerwas, *ibid.*, p. 83 and Z. Phys. **C57**, (1993) 56; and references therein.
- [18] For an overview, see J. F. Gunion, Proceeding of the 2nd International Workshop **"Physics and Experiments with Linear e^+e^- Colliders"**, eds. F. Harris, S. Olsen, S. Pakvasa and X. Tata, Waikoloa, HI (1993), World Scientific Publishing, p. 166.
- [19] J. F. Gunion and J. Kelly, hep-ph-9610421, to appear in the Proceedings of the 1996 DPF/DPB Summer Study on New Directions for High-Energy Physics; detailed results appear in preprint hep-ph-9610495.
- [20] J. Feng and T. Moroi, hep-ph-9612333.
- [21] Howard E. Haber, *Proceedings of the 21st SLAC Summer Institute on Particle Physics: Spin Structure in High Energy Process* SLAC, Stanford, CA, 26 July-6 August 1993.
- [22] Zhan XU, Da-Hua ZHANG and Lee CHANG, Nucl. Phys. **B291**, (1987) 392.
- [23] J. Werle, *Relativistic Theory of Reactions* (North-Holland, Amsterdam, 19976); A. D. Martin and T. D. Spearman, *Elementary Particle Physics* (North-Holland, Amsterdam, 1970); S. U. Chung, *Spin Formalism*, CERN Yellow Report 71-8 (1971); Martin L. Perl, *High Energy Hadron Physics* (John Wiley Sons, New York, 1974).
- [24] H. Pilkum, *The Interactions of Hadrons* (North-Holland, Amsterdam, 1967).
- [25] Peter A. Carruthers, *Spin and Isospin in Particle Physics* (Gordon and Breach, New York, 1971); M. D. Scadron, *Advanced Quantum Theory* (Springer-Verlag, Berlin, 1991).
- [26] M. L. Mangano and S. J. Parke, Phys. Rep. **200**, (1991) 301.
- [27] F. A. Berends, P. H. Daverveldt and R. Kleiss, Nucl. Phys. **B253**, (1985) 441; R. Kleiss and W. J. Stirling, Nucl. Phys. **B262**, (1985) 235; C. Mana and M. Martinez, Nucl. Phys. **B278**, (1987) 601.
- [28] J. Lorenzo Díaz-Cruz, Hong-Jian He, Tim Tai, C.-P. Yuan, Phys. Rev. Lett. **80**, (1998) 4641; M. Carena, S. Mrenna and C. E. M. Wagner, *MSSM Higgs Boson Phenomenology at the Tevatron Collider*, hep-ph/9808312v2; C. Balázs, J. Lorenzo Díaz-Cruz, Hong-Jian He, Tim Tai, C.-P. Yuan, *Probing Higgs Bosons with Large Bottom Yukawa Coupling at Hadron Colliders*, hep-ph/9807349.
- [29] A. C. Hearn, *REDUCE User's Manual*, version 3.2 (Rand Publ. CP78 Rev. 4/85, Santa Monica, CA. 1985); H. Strubbe, Comput. Phys. Commun. **8**, (1974) 1.
- [30] P. De Causmaecker, R. Gastmans, W. Troost and T. T. Wu, Phys. Lett. **B105**, (1981) 215; P. De Causmaecker, R. Gastmans, W. Troost and T. T. Wu, Nucl. Phys. **B206**, (1982) 53; F. A. Berends, R. Kleiss, P. De Causmaecker, R. Gastmans, W. Troost and T. T. Wu, Nucl. Phys. **B206**, (1982) 61; D. Dankaert, P. De Causmaecker, R. Gastmans, W. Troost and T. T. Wu, Phys. Lett. **B114**, (1982) 203; F. A. Berends, P. De Causmaecker, R. Gastmans, R. Kleiss, W. Troost and T. T. Wu, Nucl. Phys. **B239**, (1984) 382; F. A. Berends, P. De Causmaecker, R. Gastmans, R. Kleiss, W. Troost and T. T. Wu, Nucl. Phys. **B239**, (1984) 395; F. A. Berends, P. De Causmaecker, R. Gastmans, R. Kleiss, W. Troost and T. T. Wu, Nucl. Phys. **B264**, (1986) 234; F. A. Berends, P. De Causmaecker, R. Gastmans, R. Kleiss, W. Troost and T. T. Wu, Nucl.

Phys. **B264**, (1986) 265.

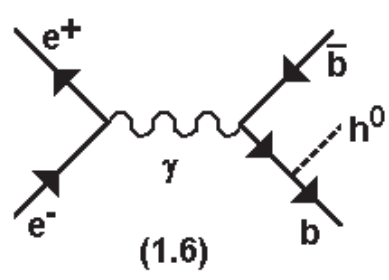
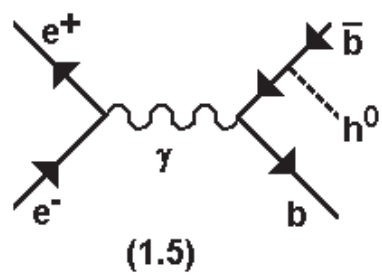
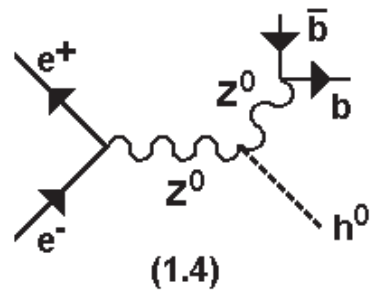
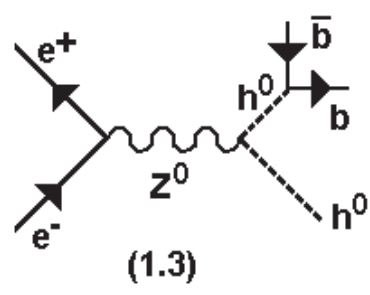
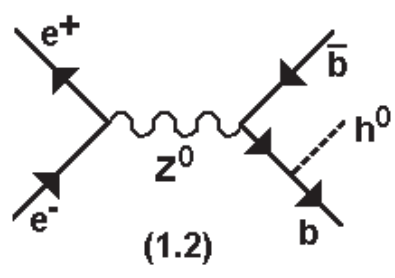
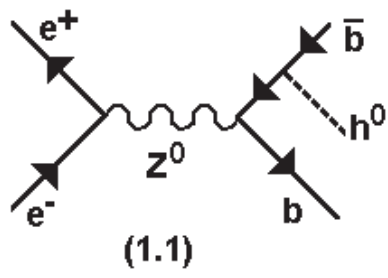


Fig. 1

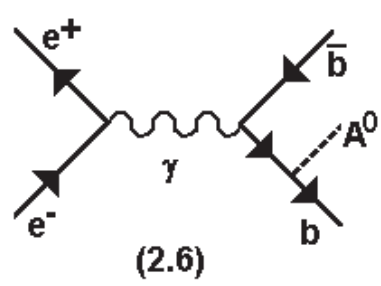
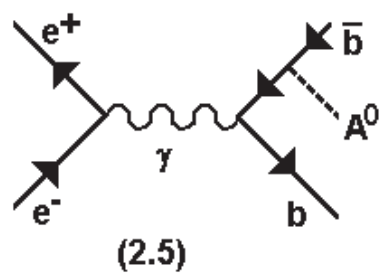
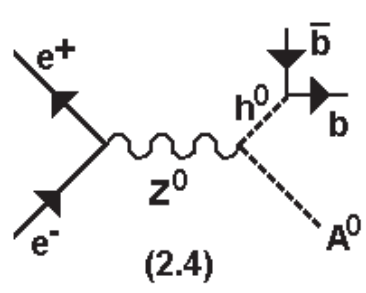
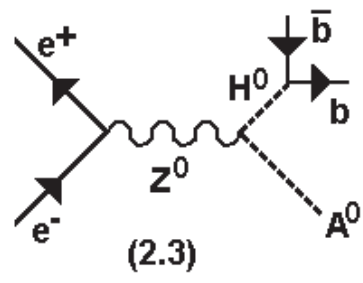
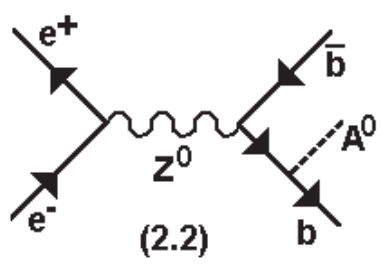
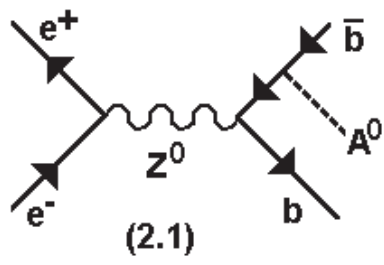


Fig. 2

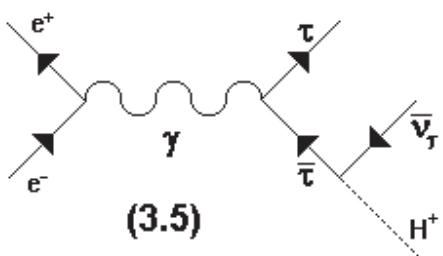
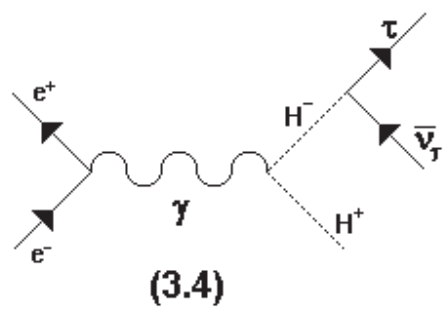
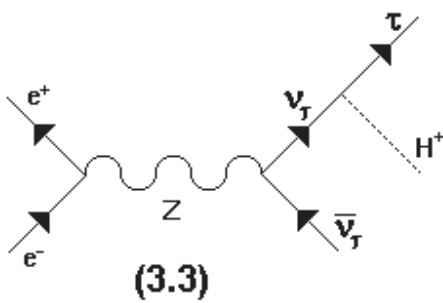
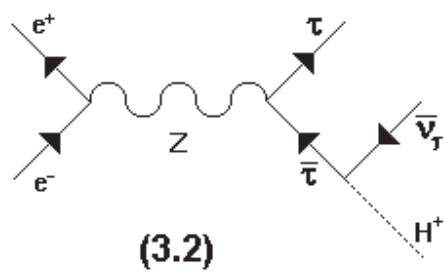
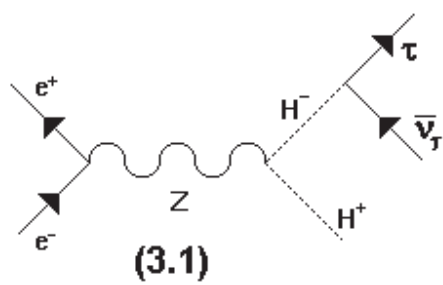


Fig. 3

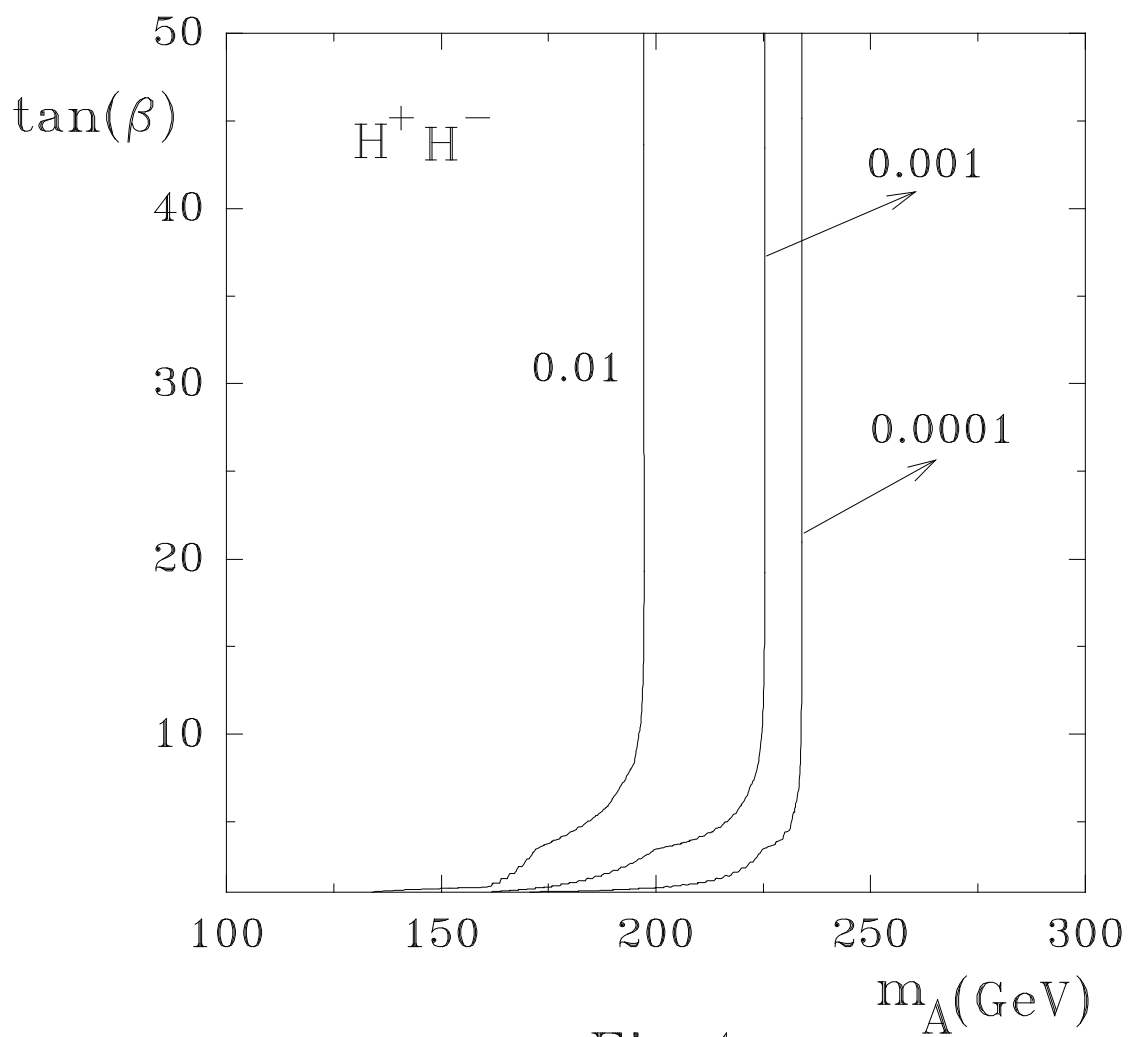


Fig.4

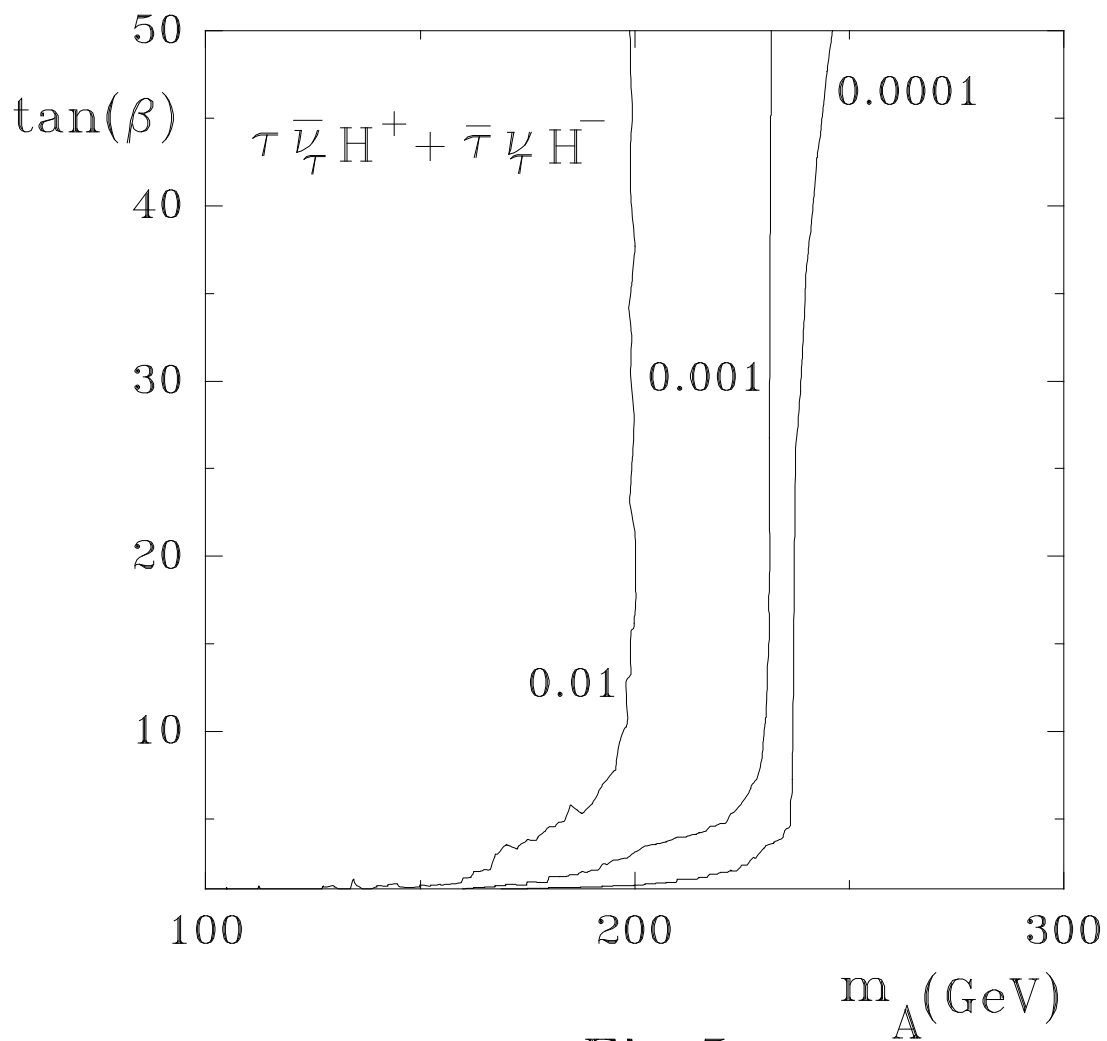


Fig.5

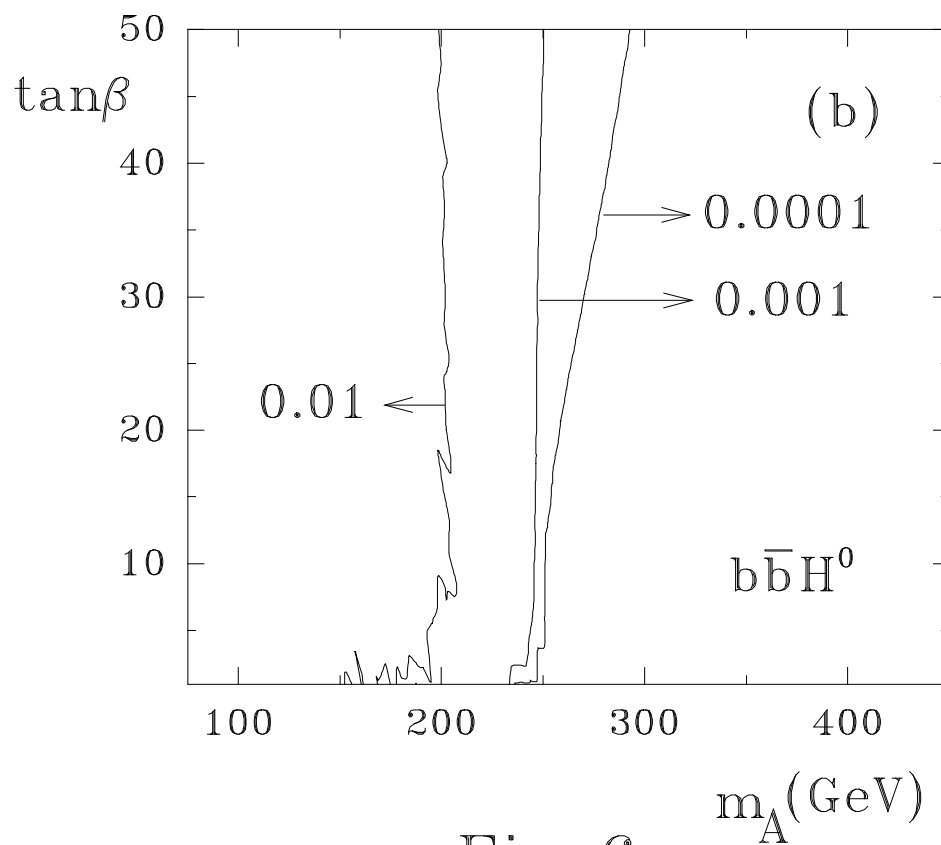
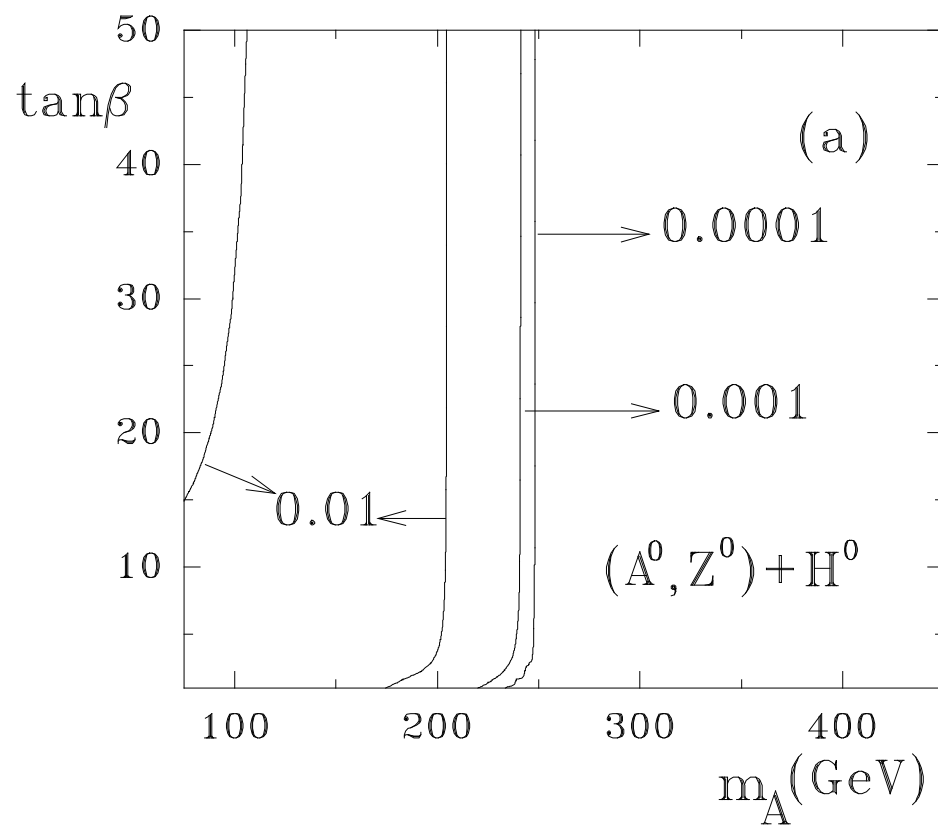


Fig 6

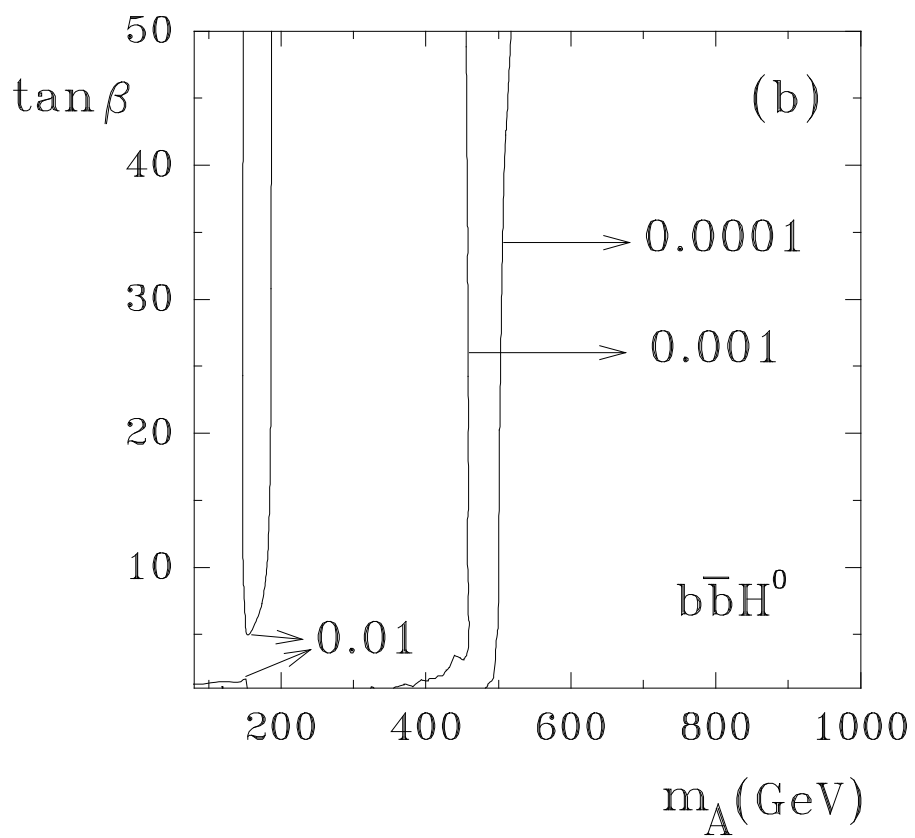
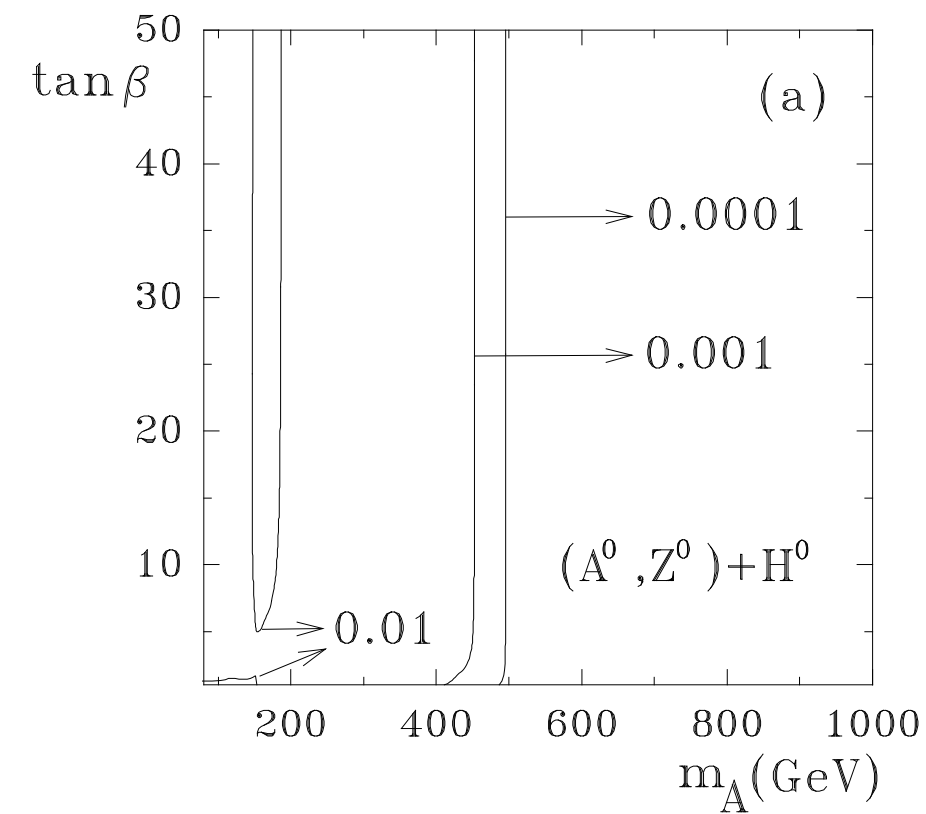


Fig. 7

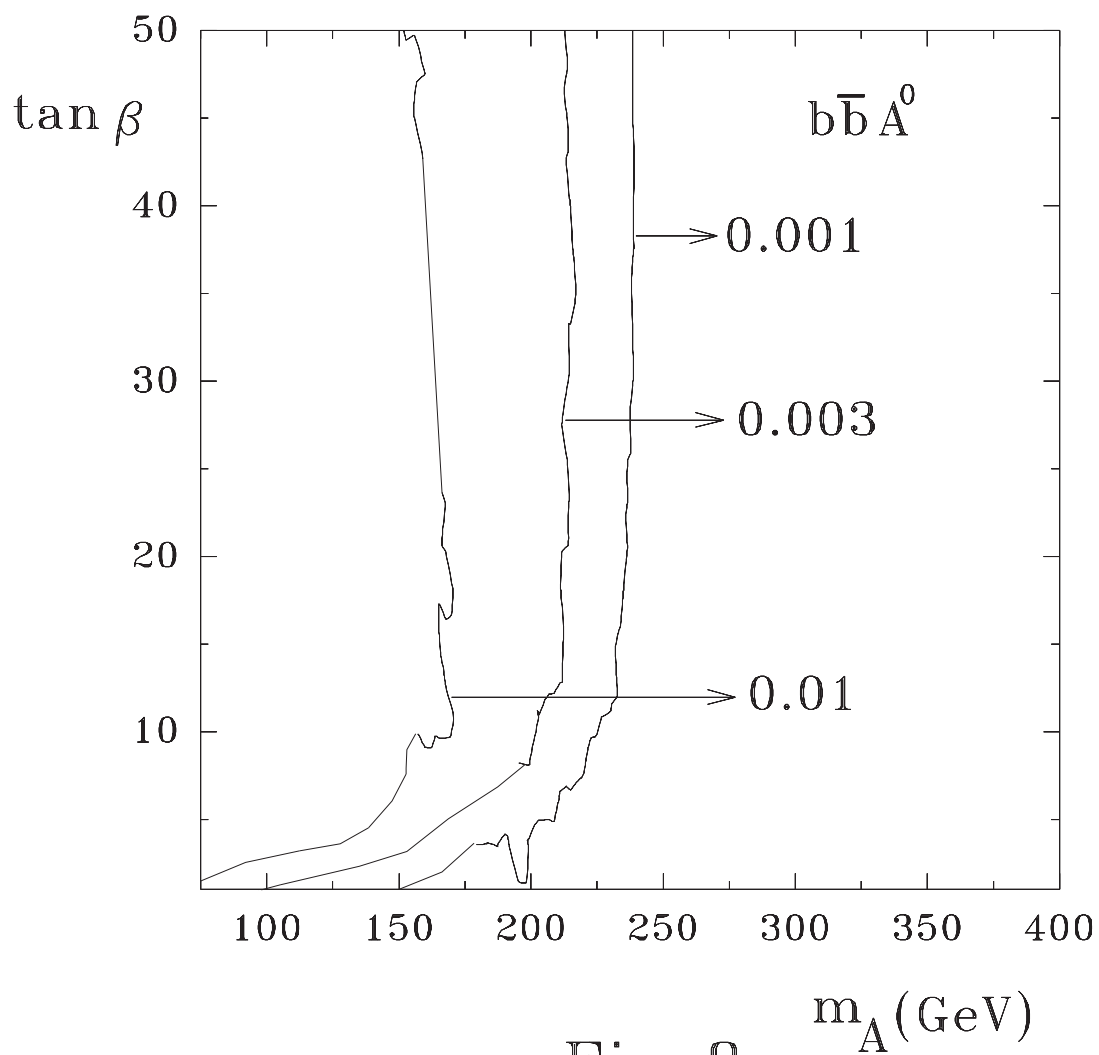


Fig 8 m_A (GeV)

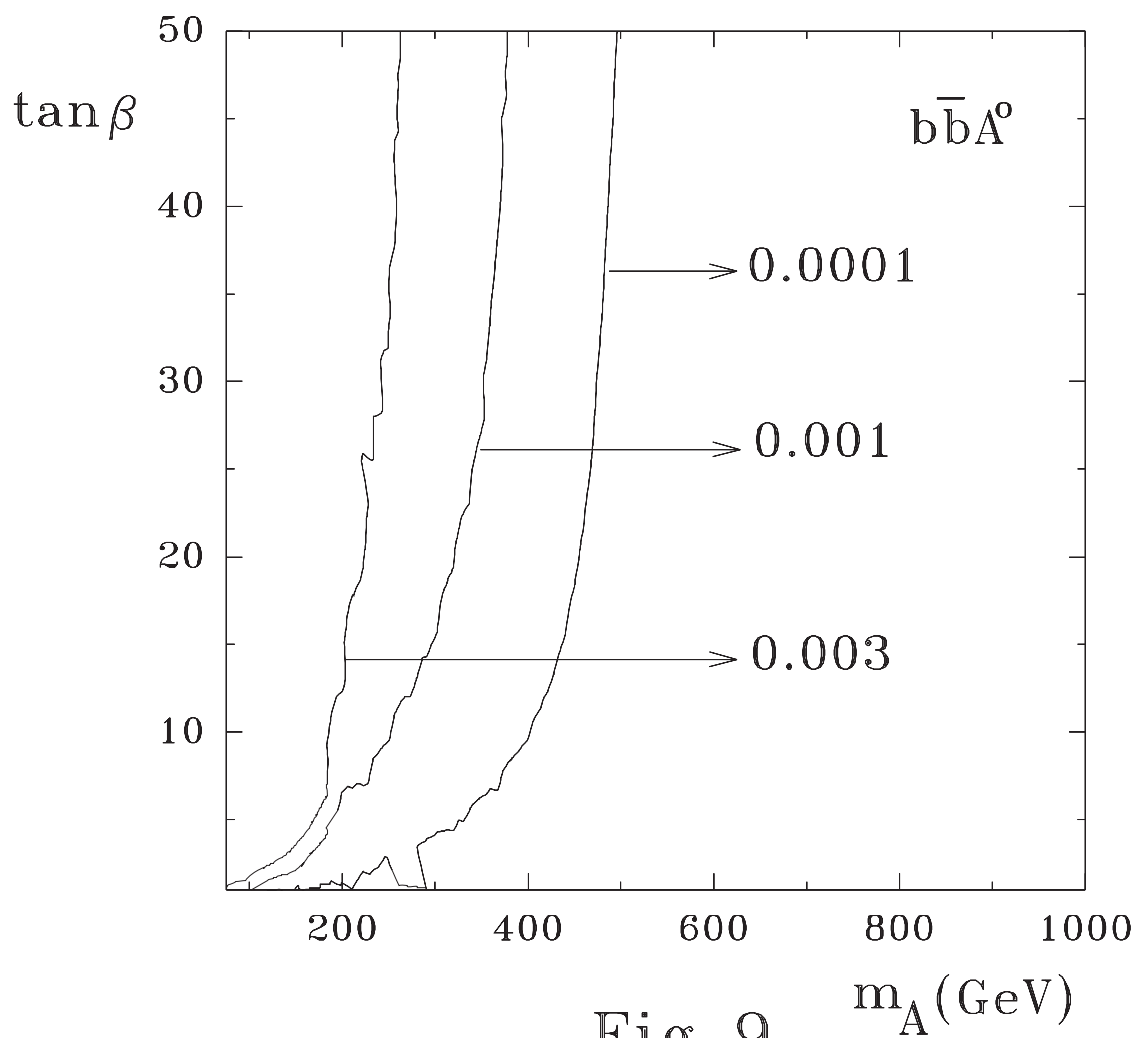


Fig 9

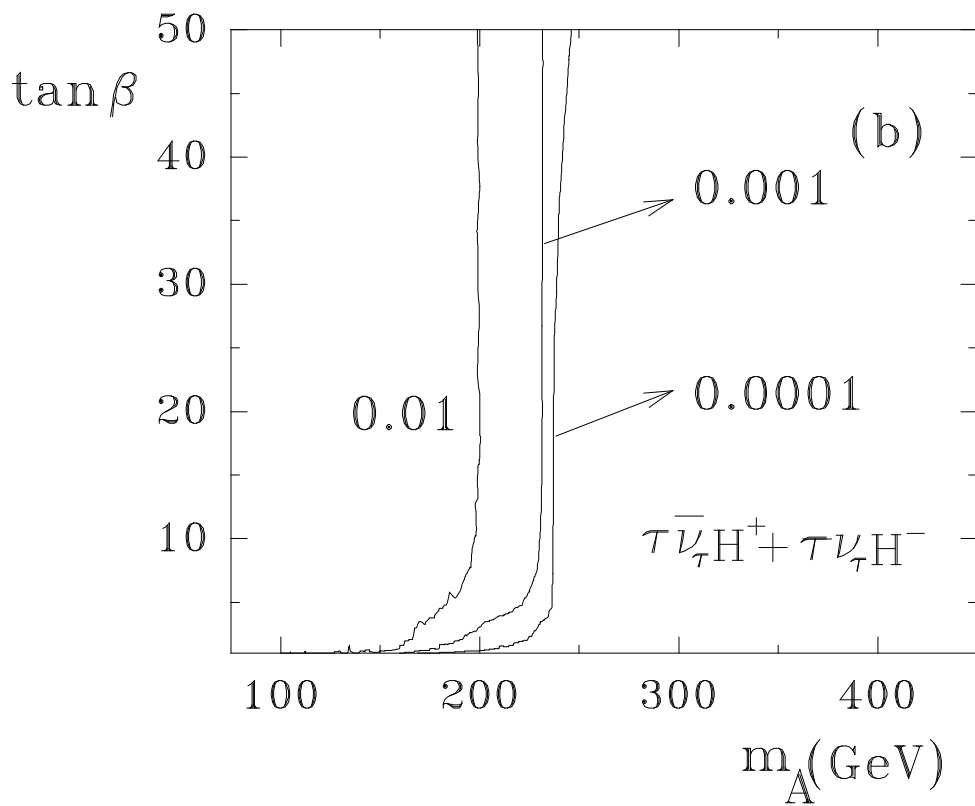
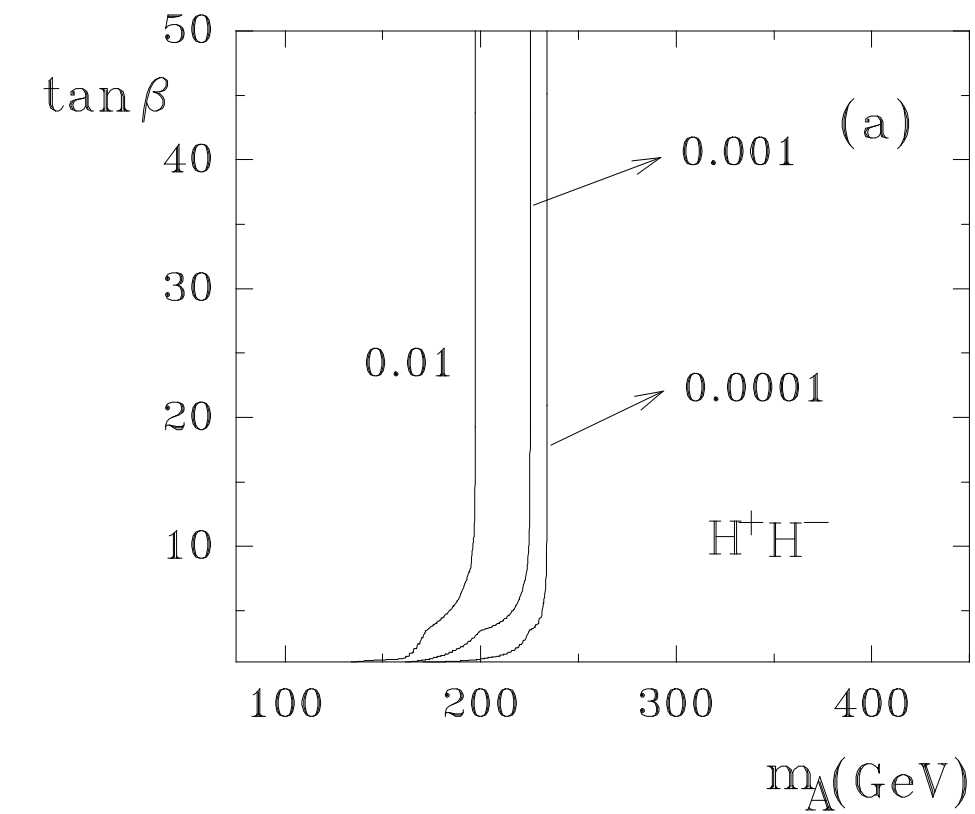


Fig 10

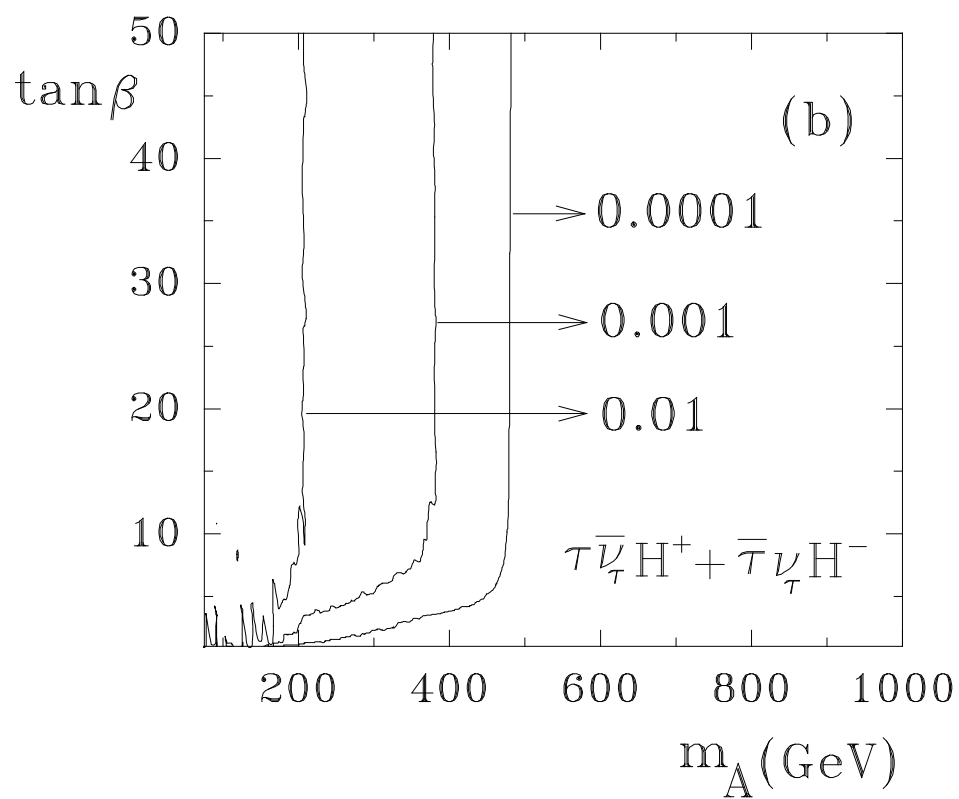
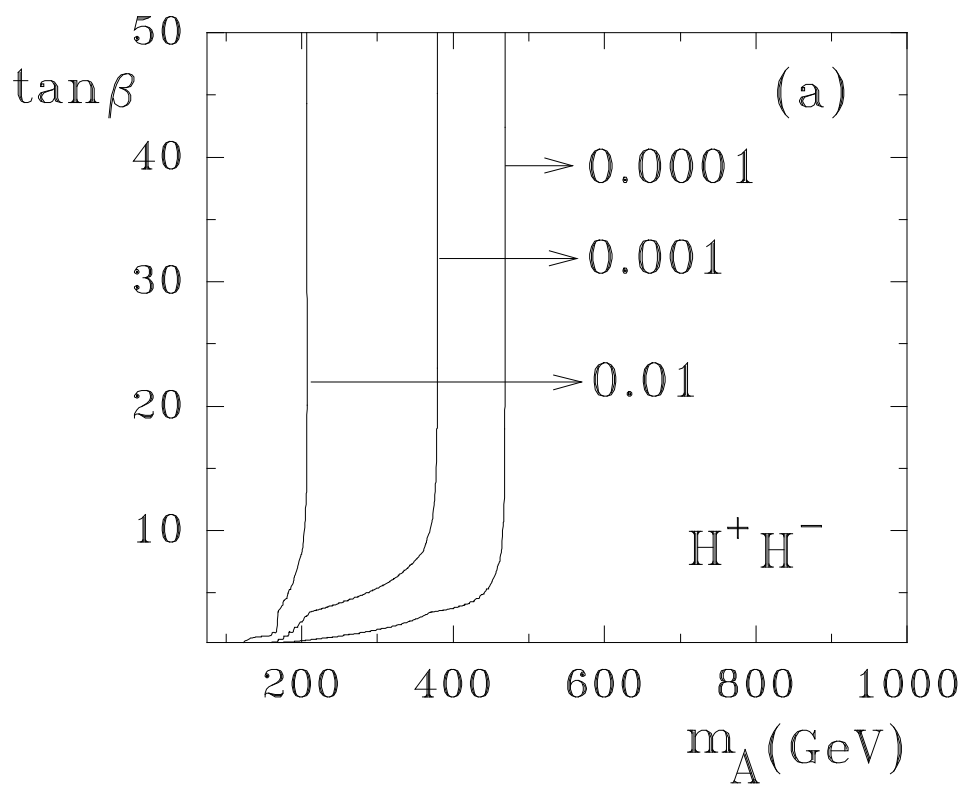


Fig 11